(Received 4 January 2025, Accepted 20 February 2025, Scheduled 18 March 2025)

The Influence of Armature Conductivity on the Propulsion Effect of Synchronous Electromagnetic Coils

Mingjie Zhong[1,2], Junsheng Cheng[1,2,*], Heyang Wang[1,2], and Jian Sun[3]

[1]*Institute of Electrical Engineering, Chinese Academy of Sciences, Beijing 100190, China*
[2]*University of Chinese Academy of Sciences, Beijing 100049, China*
[3]*Beijing Electric Power Economic and Technological Research Institute Co., Ltd., Beijing 100055, China*

ABSTRACT: In the study of synchronous electromagnetic coil launchers, the influence of armature material on system performance is critical. Existing research lacks combined simulation-experimental investigations on the electrical conductivity of armature materials and in-depth exploration of its impact mechanism on propulsion performance. To analyze the influence of armature material conductivity on propulsion characteristics, a mathematical model of the synchronous electromagnetic coil launcher was established, with theoretical derivations clarifying the mechanical properties and motion equations of the armature during acceleration. Through systematic simulations conducted on the Ansys platform, the effects of different armature material conductivities (6061 aluminum alloy, 7075 aluminum alloy, brass) on propulsion effectiveness were quantified. An experimental platform was subsequently constructed to validate simulation reliability using these three engineering-grade materials. Results demonstrate that increased armature conductivity significantly reduces peak reverse force and enhances exit velocity, while revealing a saturation effect: when conductivity exceeds 6×10^7 S/m, further improvements have diminishing returns on propulsion performance.

1. INTRODUCTION

In the field of electromagnetic propulsion, coil electromagnetic launchers have garnered significant attention due to their simple structure, flexible design, high acceleration efficiency, and substantial electromagnetic thrust [1–3]. Compared to other electromagnetic launchers, coil electromagnetic launchers operate without physical contact between the drive coil and transmitting coil [4], a feature that improves their reliability and performance from the structural aspect [5, 6]. According to the different modes of operation, coil electromagnetic thrusters can be divided into two types: synchronous and asynchronous [7]. The operating principle of synchronous coil electromagnetic thruster is to induce eddy currents in the armature through the time-varying magnetic field generated by the driving coil [8], and then generate electromagnetic force through the interaction between the current and time-varying magnetic field, so as to accelerate the armature [9]. The asynchronous coil electromagnetic thruster exhibits a high presence of negative and zero-sequence components in experiments, leading to low efficiency and making practical application difficult [10].

In the pulse circuit structure, Zhang et al. [11] proposed an improved topology for the main circuit disconnection, pry bar disconnection circuit, and pry bar circuit with inductance, all of which enhanced energy conversion efficiency to some extent. Ram and Thomas [12] utilized a thyristor-based driving coil current switching circuit, effectively reducing the armature capture effect through commutation.

In terms of software and algorithm optimization, Citak et al. [13] used Delphi software to adjust the triggering time of the coil to improve the initial speed and optimize system performance. Niu et al. [14, 15] applied adaptive design strategies to the triggering timing control design of multi-stage synchronous induction coil thrusters.

Regarding material and structural optimization, Lu et al. [16] proposed a new step-type Synchronous Induction Coilgun (SICG) by altering the structure of the driving coil and armature, further reducing the impact of the system's inherent characteristics on performance and improving acceleration efficiency. Ram and Thomas [17] analyzed the effect of induced currents when hollow armatures of different lengths move within a multi-stage eddy current generator.

Based on the large impact of the armature on the performance of the propulsion system, the attention of many scholars has been focused on armature. Ref. [18] explored the change rule of equivalent inductance and equivalent resistance at all levels when the armature position of a three-stage synchronous induction coil transmitter was changed.

Ref. [19] starts from the inherent parameters of the armature and uses simulation methods to modify these parameters, observing the variation of magnetic flux density in the armature bore. However, most studies have only simulated armatures made of copper and aluminum, which introduces significant uncertainty due to the limited choice of two materials with different conductivities. This approach does not provide a concrete understanding of the underlying influence mechanisms. Furthermore, no actual experiments have been conducted to validate the simulation results. Given that armature is a critical

* Corresponding author: Junsheng Cheng (jscheng@mail.iee.ac.cn).

component of a synchronous induction coil launcher and has a substantial impact on the overall system's launch efficiency, further in-depth exploration is necessary.

This paper investigates the effect of armature conductivity on exit velocity and reverse force using the finite element method. To further analyze its influence, simulations are conducted with armatures of the same resistance but different materials. The results are validated through experiments to confirm the accuracy of the simulation.

2. SYNCHRONOUS INDUCTION COIL ELECTROMAGNETIC LAUNCHER

2.1. Principle of Single-Stage Synchronous Induction Coil Electromagnetic Launcher

The synchronous induction coil electromagnetic launcher operates based on the magnetic coupling principle between the driving coil and armature, and can be essentially understood as a linear motor [20]. The basic structure of this launcher includes a driving coil, armature, switch, power supply, etc. Its outer body can be composed of one or more driving coils, similar to the stator part of a motor, while the armature can be regarded as the rotor of the motor [21]. The simplified working principle diagram is shown in Figure 1. When the pulsed power supply is discharged at the corresponding time, the driving coil is discharged; there will be a changing magnetic field around it, causing the armature coil to sense a current; and finally the magnetic field generated by the combined effect of the sensed current and the driving coil current pushes the armature forward until the armature leaves the launcher [22].

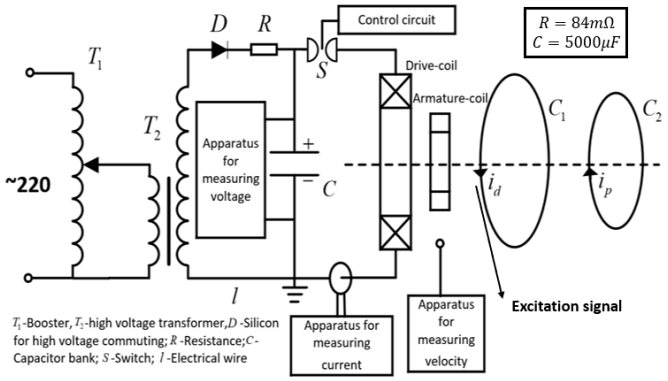

FIGURE 1. Schematic diagram of the working principle of a single-stage synchronous induction coil electromagnetic launcher.

2.2. Analysis of Armature Motion Process

In the synchronous induction coil launcher, under the influence of the axial magnetic field, the armature surface only experiences induced currents along the circumferential direction. The moving metal cylindrical armature is modeled as consisting of numerous mutually independent current loops, as illustrated in Figure 2.

Without considering the microscopic characteristics of the armature and the low requirement for calculation accuracy, each current equivalent to the entire armature can be viewed as a single turn coil, which is a series lumped parameter circuit model composed of a coil and a resistor. After applying current to the driving coil, the equivalent current loop of the armature will also induce current. Under the action of a magnetic field, this current will generate an axial thrust, accelerating the forward movement of the armature.

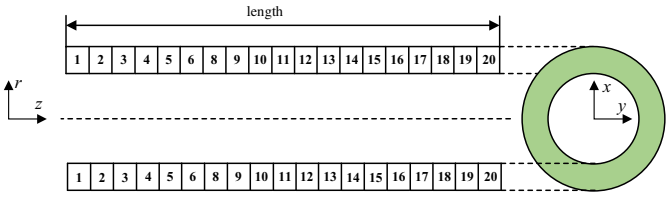

FIGURE 2. Armature current loop model.

According to Ampere's law of force, the axial force on the armature can be obtained as:

$$F_z = -i_p 2\pi r B_r^d \tag{1}$$

Among them, i_p is the current of the armature current loop, r the radius of the armature current loop, and B_r^d the radial magnetic field component generated by the driving coil on the armature.

Therefore, the axial thrust of the entire armature is:

$$F_z = -\sum_{i=1}^{N_d}\sum_{j=1}^{N_p} i_i^d i_j^p \frac{dM_{i,j}}{dz} \tag{2}$$

The axial velocity of the armature is:

$$v = v(0) + \int_0^t F_z/m_p dt = \frac{dz}{dt} \tag{3}$$

Among them, a is the acceleration of the armature, F_z the axial force on the armature, m_p the mass of the armature, v the armature speed, $v(0)$ the initial velocity of the armature, t the time, and z the axial displacement.

The efficiency of promotion can be expressed as:

$$\eta = \frac{W_p}{W_c} = \frac{\frac{1}{2}mv_p^2 - \frac{1}{2}mv_0^2}{\frac{1}{2}CU^2} \tag{4}$$

Among them, $\frac{1}{2}CU^2$ is the capacitor energy storage, m the armature mass, v_p the outlet velocity, v_0 the inlet velocity of the armature, U the voltage value of the energy storage power supply, and C the capacitance of the energy storage power supply.

3. FINITE ELEMENT SIMULATION ANALYSIS OF ARMATURE DURING THE PROPULSION PROCESS

In this paper, the simulation test is carried out in Ansoft finite element simulation platform, and the pulse capacitor is used to supply power to the driving coil. The specific parameter values selected can be seen in the Table 1, and the simulation time is set to 6 ms. In the process of finite element simulation, part

TABLE 1. Simulation parameters.

Component name	Parameter	Value
Power supply	Capacitance value (μF)	5000
	Capacitor initial voltage (kV)	4
Drive coil	Coil inner diameter (mm)	62.5
	Turns	60
	Coil length (mm)	80
Armature	Armature outer diameter (mm)	58
	Armature thickness (mm)	10
	Armature mass (kg)	5

of the idealisation is carried out, and it is assumed that there is no friction between the armature and propellers and that the air resistance has no effect on the armature during the acceleration process.

In order to simplify the model and facilitate the analysis, the simulation model is simplified to consist of a driving coil and an armature, as shown in Figure 3. The influence of external factors such as the shell on the propulsion process is ignored, and this simplification makes the study more focused on the core electromagnetic effect.

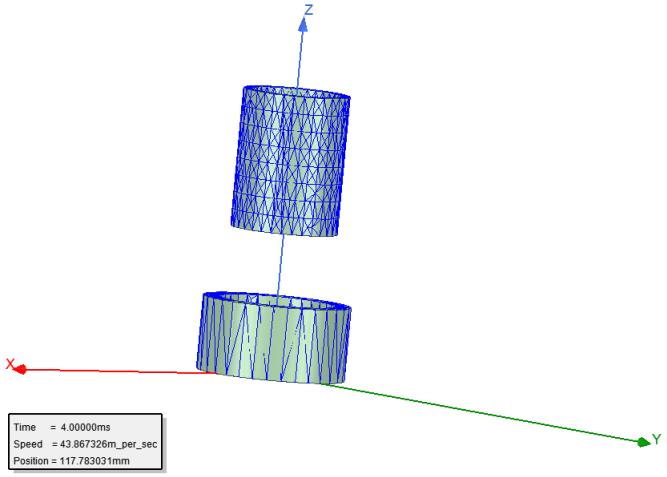

FIGURE 3. Schematic diagram of the simulation model.

4. FINITE ELEMENT SIMULATION ANALYSIS OF CONDUCTIVITY OF DIFFERENT ARMATURE MATERIALS

The strength of the induced eddy currents in an armature depends mainly on the conductivity of its material (σ) and the rate of change of the magnetic field ($\frac{dB}{dt}$). When σ is increased, the Lorentz force in the armature is enhanced by increasing the induced current strength per unit volume (J) with the same change in magnetic field.

The component of the Lorentz force along the axial direction is the thrust of the armature forward motion, so increasing the armature conductivity will directly increase the axial driving force of the armature, and thus increase the armature exit velocity.

During the entire acceleration process, the eddy currents induced in the armature exhibit a more pronounced skin effect phenomenon. When calculating the equivalent resistance of the armature, the induced eddy currents are predominantly distributed on its surface. Consequently, the skin depth is set as:

$$\delta = \sqrt{\frac{2}{2\pi f \mu \sigma}} \tag{5}$$

where f is the pulse current frequency (Hz), σ the armature material conductivity ($S \cdot m^{-1}$), and μ the armature material permeability.

Through the analysis of the above equation, it can be found that after controlling the pulse current frequency to a fixed value, the skinning depth is only related to the conductivity and magnetic permeability of the armature material. Non-magnetic materials are typically selected for armatures to ensure a magnetic permeability close to 1. During the acceleration process, the skinning depth significantly affects the exit velocity and force of the armature. Therefore, this paper further explores the effect of different armature conductivities on armature performance.

In order to exclude the influence of other factors, the armature is set not to deform, and the thermal effect is ignored in the simulation. The conductivity range is set as $0 \sim 10 \times 10^7$ S/m, which covers the conductivity of metals commonly used in industry, and the effect of armature conductivity on armature acceleration is further explored with several sets of simulation experiments. The simulation results were then analyzed through MATLAB charts, and curve fitting was performed for the relationship between conductivity and armature exit velocity and peak reverse force as shown in Figure 4.

From Figure 4, it can be seen that there is a positive correlation between armature exit velocity and conductivity. In the range from 2.5×10^6 S/m to 10×10^7 S/m, the armature ve-

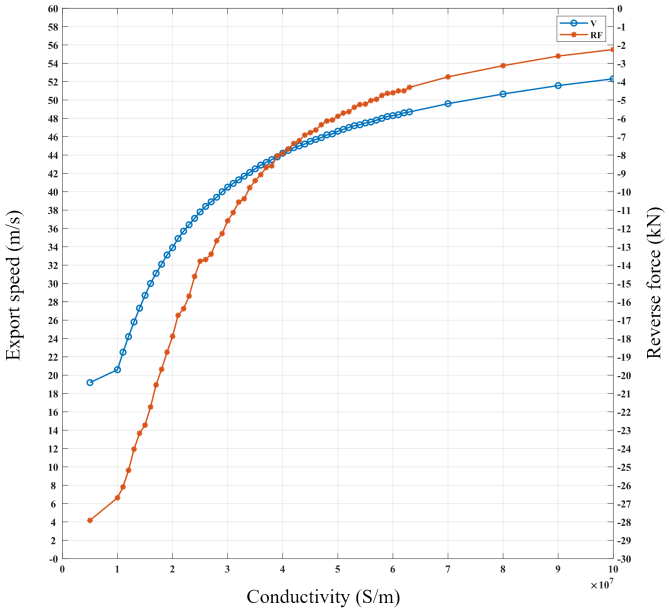

FIGURE 4. Curve of armature conductivity versus exit velocity and peak reverse force.

locity increases with increasing conductivity, but the growth rate slows down gradually. When the conductivity increases to 6×10^7 S/m, the effect of continuing to increase the conductivity on the exit velocity is no longer significant.

In order to further verify the simulation results, several engineering materials commonly used in armature manufacturing, such as 6061 aluminium alloy, 7075 aluminium alloy, and brass, are selected in this paper to analyze the relationship between the conductivity and exit velocity, and the simulated values are compared with the experimental ones, as shown in Table 2. Three armature materials (6061 aluminum alloy, 7075 aluminum alloy, and brass) were selected due to their superior integrated electromagnetic-mechanical properties. Specifically, 6061 aluminum alloy offers cost-effectiveness, moderate electrical conductivity, and notable fatigue resistance; 7075 aluminum alloy is characterized by high specific strength, meeting the demands of high acceleration conditions; and brass exhibits excellent wear resistance and thermal stability under sliding contact conditions. In selecting the armature material, one can also consider purple copper armature as it has high electrical conductivity and is easier in the armature manufacturing process.

TABLE 2. Export speeds corresponding to different armature materials.

Armature material	Conductivity (S/m)	Curve exit speed (m/s)	Simulated exit velocity (m/s)
6061 Aluminium Alloy	3.600×10^7	42.9	42.94
7075 Aluminium Alloy	2.633×10^7	38.55	38.60
Brass	1.61×10^7	30.1	30.16

Table 2 shows that the exit velocity of the armature material read directly from the relationship curve is very close to the simulation results, verifying the correctness of the relationship curve. Figure 4 also shows that the conductivity also shows a positive correlation with the peak armature reverse force in general.

While in the range of $5 \times 10^6 \sim 10 \times 10^7$ S/m, the peak reverse force increases with increasing conductivity, and the rate of increase of the peak reverse force decreases with further increase in conductivity. When the conductivity reaches 6×10^7 S/m, further increase in conductivity has less effect on the peak reverse force. Theoretically, the magnitude of the induced eddy currents is limited by the rate of change of the magnetic field ($\frac{\mathrm{dB}}{dt}$), which itself is limited by the maximum capacity of the driving coil current.

As the conductivity continues to increase, the rate of change of flux that can be supplied by the drive coil itself has reached the limit of the physical conditions even if the induced current is continually increased, resulting in a diminished effect of further enhancement. The phenomenon of high conductivity saturation arises from the electromagnetic field-current coupling dominated by the skin effect. When the armature conductivity (σ) exceeds the critical value ($\sigma_c = \frac{2}{\mu\omega L^2}$), the skin depth ($\delta \propto \sigma^{-1/2}$) significantly decreases, causing the current distribution to be confined to the surface (effective conductive cross-sectional area $A_{eff} \propto \delta \cdot L \propto \sigma^{-1/2}$). At this point, the nonlinear increase in the skin resistance ($R_{skin} \propto \sqrt{\sigma}$) suppresses the rise in current density ($J \propto \sigma^{-1/2}$), thereby limiting the electromagnetic force density ($f = J \times B \propto \sigma^{-1/2}$) and acceleration ($a \propto \sigma^{-1}$).

The increase in velocity increment Δv with σ exhibits a logarithmic saturation property ($\Delta v \propto \int \sigma^{-1} dt \propto \ln \sigma$), indicating that when $\sigma \gg \sigma_c$, the further increase in conductivity has a diminishing marginal contribution to propulsion performance.

The peak armature reverse forces corresponding to different armature materials were produced following Table 2 as shown in Table 3.

TABLE 3. Peak reverse force corresponding to different armature materials.

Armature material	Conductivity (S/m)	Curve value (kN)	Simulation value (kN)
6061 Aluminium Alloy	3.600×10^7	-9.0727	-8.8715
7075 Aluminium Alloy	2.633×10^7	-13.7988	-13.5322
Brass	1.61×10^7	-21.7420	-21.5330

Similarly, Table 3 shows the peak reverse force corresponding to different armature materials, which is consistent with the simulation results and further verifies the accuracy of the relationship curves.

5. TEST VALIDATION

In the previous section, theoretical analyses and simulations were performed to investigate how the armature conductivity affects the acceleration process, and several relationships were identified. To further verify these theoretical findings, a single-stage induction coil propulsion system was constructed, and corresponding experimental validations were conducted. The system specifically includes a charger, a capacitor bank, a vacuum switch, a renewing diode, a single-stage induction coil launcher, a cylindrical armature, and a light curtain speed measurement system. The working principle is as follows: First, the capacitor bank is charged to a preset voltage using the charging machine. After reaching this set voltage, the charging switch is disconnected. Then, the control system outputs a pulse signal to trigger the vacuum switch, activating the single-stage coil. When the armature coil reaches a certain speed, it sequentially passes through the front and rear light curtains. By recording the time taken for the armature coil to pass between these two light curtains and knowing the distance between them, the exit velocity of the armature coil can be calculated.

The relationship of the experimental system is shown schematically in the Figure 5.

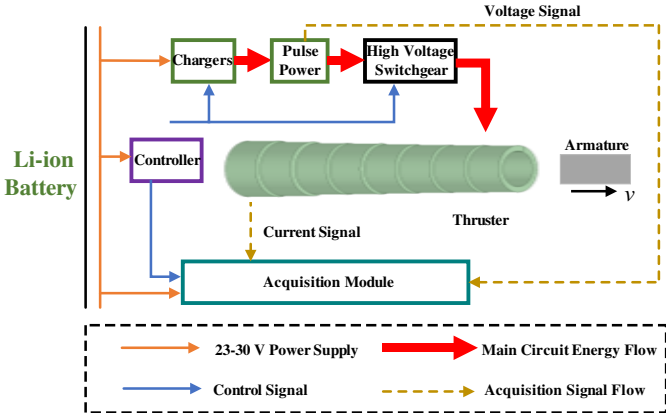

FIGURE 5. Schematic diagram of the synchrocoil propulsion.

Three armature materials were selected for this experiment, namely: 6061 aluminium alloy, 7075 aluminium alloy, and brass. For armatures with a total mass of 5 kg, no additional counterweight is required. However, if the armature mass is less than 5 kg, epoxy resin is used as the counterweight material to achieve the target mass. Its physical diagram is shown in Figure 6. The hardware model and measurement system are shown in Figure 7. The experimental results under different armature materials are given in Table 4.

By comparing the actual exit speed of the armature measured experimentally with the simulation results, although there is a certain error, the error is within the acceptable range (no more than 10%, which meets the requirements of engineering applications). The experimental speed is slightly lower than the simulation speed, but the trends of the two are consistent with the conclusions of the theoretical derivation and simulation analysis. The reasons for the error may include:

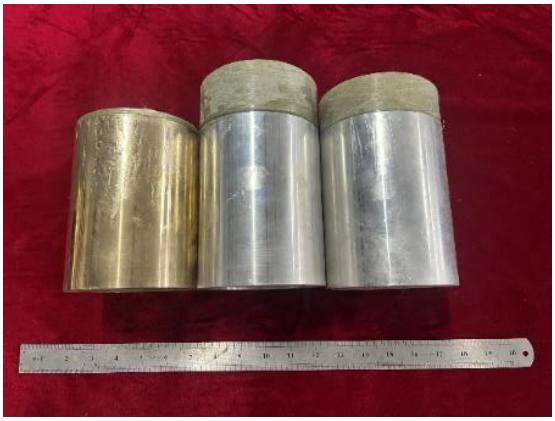

FIGURE 6. Physical drawing of armature with different materials.

FIGURE 7. Hardware model and measurement system.

TABLE 4. Comparison of experimental and simulation data.

Armature material	Conductivity (S/m)	Simulated exit velocity (m/s)	Actual exit velocity (m/s)	Relative error (%)
6061 Aluminium Alloy	3.600×10^7	42.94	40.45	6.15
7075 Aluminium Alloy	2.633×10^7	38.60	35.67	8.21
Brass	1.61×10^7	30.16	29.85	1.03

(1) The actual experimental conditions may not fully replicate the ideal settings used in the simulation, such as armature deformation during acceleration, and thermal effects on the drive coil and armature must not be overlooked.

(2) Friction between the armature and driving coil structure during acceleration, as well as precision errors in the device fabrication, may also influence the experimental results.

(3) The accuracy of armature conductivity measurements can be affected by the measurement instruments and methods used, potentially leading to discrepancies with the true value.

6. CONCLUSION

This study shows, through finite element simulation and experimental studies, that the conductivity of the armature material has a significant effect on the acceleration performance of the thruster. Through finite element simulation and experimental studies, it was found that increasing armature conductivity significantly reduces the peak reverse force and enhances the armature exit velocity.

In addition, the induced eddy currents are primarily concentrated in the rear and outer regions of the armature, due to the high rate of magnetic field change and the pronounced skin effect in these areas. Conversely, the magnetic field near the front and inner surfaces of the armature is more uniform, with slower flux variations, resulting in weaker induced eddy currents. These phenomena highlight the complex interaction between the armature and the magnetic field in an electromagnetic emission system, which is a critical consideration for design and optimization.

In practical design, a balance must be found among conductivity, mechanical properties, and cost, with the selection of appropriate materials and parameters to optimize electromagnetic propulsion performance.

Future work will focus on investigating the microscopic electromagnetic properties of different armature materials, expanding material combinations for optimized propulsion performance, and developing a multi-parameter optimization model. Additionally, the dynamic coupling between the armature and magnetic field will be explored to enhance the stability and reliability of the propulsion system.

REFERENCES

[1] Shi, J., X. Guan, S. Guan, and B. Wu, "Missile-borne storage testing technology research of synchronous induction coil launcher," *Transactions of China Electrotechnical Society*, Vol. 39, No. 2, 325–332, 2024.

[2] Ma, W., J. Lu, and Y. Liu, "Research progress and challenges of electromagnetic launch technology," *Transactions of China Electrotechnical Society*, Vol. 38, No. 15, 3943–3959, 2023.

[3] Wang, Q., H. Wang, X. Li, and S. Chen, "Review of coaxial coil electromagnetic propulsion technology," *High Voltage Engineering*, Vol. 41, No. 08, 2489–2499, 2015.

[4] Cao, Y., W. Liu, R. Li, Y. Zhang, and B. Zou, "Study of discharge position in multi-stage synchronous inductive coilgun," *IEEE Transactions on Magnetics*, Vol. 45, No. 1, 518–521, 2009.

[5] Guan, S., X. Guan, B. Wu, and J. Shi, "Analysis of the influence of system parameters on launch performance of electromagnetic induction coil launcher," *Energies*, Vol. 15, No. 20, 7803, 2022.

[6] Guo, D. H., D. L. Shi, X. C. Guan, S. H. Guan, and B. Wu, "Simplification of capacitance driven multistage coilgun model," *Electric Machines and Control*, Vol. 26, No. 5, 9, 2022.

[7] Guan, X., L. Yuan, and S. Guan, "Research on electromechanical model of multistage synchronous induction launcher," *IEEJ Transactions on Electrical and Electronic Engineering*, Vol. 17, No. 12, 1783–1789, 2022.

[8] Qian, H., Z. Sun, W. Xu, F. Cui, and C. Cao, "Performance optimization on multiple-stage synchronous induction coil launcher considering hindrance effect," *IEEE Transactions on Applied Superconductivity*, Vol. 31, No. 8, 1–4, 2021.

[9] Zhang, T., W. Guo, Z. Su, Y. Liu, and W. Fan, "Analysis of improving efficiency on synchronous induction coilgun based on the directional change of magnetic field," *Transactions of China Electrotechnical Society*, Vol. 36, No. 03, 517–524, 2021.

[10] Liu, K., Z. Xiao, X. Niu, and Y. Zhang, "Research of varying frequency driving scheme for asynchronous induction coil launcher," *IEEE Transactions on Plasma Science*, Vol. 45, No. 7, 1567–1573, 2017.

[11] Zhang, Y., Y. Gong, M. Xiong, Q. Bao, X. Niu, and X. Li, "Research on driving circuit improvement of coilgun," *IEEE Transactions on Plasma Science*, Vol. 47, No. 5, 2222–2227, 2019.

[12] Ram, R. and M. J. Thomas, "A novel technique to arrest the armature capture effect in an induction coilgun," *IEEE Transactions on Plasma Science*, Vol. 50, No. 10, 3334–3340, Oct. 2022.

[13] Citak, H., Y. Ege, and M. Coramik, "Design and optimization of delphi-based electromagnetic coilgun," *IEEE Transactions on Plasma Science*, Vol. 47, No. 5, 2186–2196, 2019.

[14] Niu, X., K. Liu, Y. Zhang, Z. Xiao, and Y. Gong, "Research on adaptive design of multi-stage synchronous induction coil launcher," *Transactions of China Electrotechnical Society*, Vol. 33, No. 15, 3644–3650, 2018.

[15] Niu, X., K. Liu, Y. Zhang, Z. Xiao, G. Xiao, and Y. Gong, "Research on self-consistent control strategy of multistage synchronous induction coil launcher," *Energy*, Vol. 144, 1–9, 2018.

[16] Lu, F., Y. Wang, Z. Yan, Y. Hu, and H. Deng, "Investigation of the inner conical armature in synchronous induction coilgun," *IEEE Transactions on Plasma Science*, Vol. 47, No. 8, 4203–4208, 2019.

[17] Ram, R. and M. J. Thomas, "Effect of mutual magnetic flux linkage between stages of an induction coilgun on its performance," *IEEE Transactions on Plasma Science*, Vol. 50, No. 7, 2285–2292, Jul. 2022.

[18] Zhao, K., X. Yuan, H. Xiang, Q. Zhan, and Q. Lv, "Measurement and analysis of equivalent impedance for three-stage synchronous induction coil launcher," in *Journal of Physics: Conference Series*, Vol. 1074, No. 1, 012091, 2018.

[19] Guan, S., X. Guan, B. Wu, *et al.*, "Analysis of effects on in-bore magnetic field distribution characteristic of multi-stage SICL armature," *Journal of Naval University of Engineering*, Vol. 35, No. 03, 22–28, 2023.

[20] Lu, J. Y. and Y. Q. Liu, "Review on linear motor for electromagnetic launch and its control technology," *Transactions of China Electrotechnical Society*, Vol. 39, No. 19, 5899–5913, 2024.

[21] Li, W., S. D. Li, S. L. Liu, L. Xiong, and J. S. Cheng, "Analysis of dynamic mechanical state of electromagnetic synchronous induction coils during propulsion," *Journal of Weapons and Equipment Engineering*, Vol. 44, No. 5, 157–164, 2023.

[22] Zheng, F. Z., C. B. Huang, R. X. Jiang, M. K. Lu, and H. N. Qian, "Analysis and optimization method of the influence of power mode on the performance of a multi-stage synchronous induction coil," *Journal of Weapons and Equipment Engineering*, Vol. 43, No. 12, 165–171, 2022.